Thin–Walled Structures 205 (2024) 112409

Contents lists available at ScienceDirect

Thin-Walled Structures

journal homepage: www.elsevier.com/locate/tws

Negative Poisson's ratio can enhance stability of layered composite structures

Wenhua Lin, Yeqing Wang *, Barry D. Davidson

Department of Mechanical & Aerospace Engineering, Syracuse University, Syracuse, NY 13244, United States

ARTICLE INFO

Keywords:
Auxetic composite laminates
Negative Poisson's ratio
Critical buckling strength
Bending stiffness matrix
Homogeneous monoclinic plate

ABSTRACT

Composite laminates with negative Posson's ratios (*i.e.,* auxetic composite laminates) were experimentally found to demonstrate a three-fold increase in buckling strength under uniaxial compression in comparison with the equivalent non-auxetic ones. To investigate whether the enhancement is genuinely due to the negative Poisson's ratio (*i.e.,* the auxeticity) or merely caused by the concurrent change in the bending stiffness matrix as the composite layup changes, a novel monoclinic plate-based composite laminate approach is proposed, which for the first time, allows to isolate the auxeticity effect from the concurrent change of the stiffness matrix. Results provided theoretical proof that the auxeticity plays an active role in enhancing the critical buckling strength of layered composite structure. However, such a role is dynamically sensitive to elements in the bending stiffness matrix, especially the bending-twisting ratio and the anisotropy of the bending stiffness between the longitudinal and lateral directions. Insights are expected to provide guidance in exploiting negative Poisson's ratio for improving the stability of layered composite structures.

1. Introduction

A material with one or more negative Poisson's ratios is referred to as auxetic [1-4]. For carbon fiber reinforced polymer (CFRP) matrix composite laminates, which is a popular class of layered composite structures used in aerospace, automotive, marine, infrastructure, etc., auxeticity can be introduced into the laminates by tailoring the layup [5, 6]. Much of the interest in auxetic composite laminates arises due to their improved impact and indentation resistance capabilities [7-14]. For instance, Aziz [15] reported that for auxetic and equivalent non-auxetic CFRP composite laminates with similar longitudinal moduli of 64.8 and 61.7 GPa, respectively, and in-plane Poisson's ratios of −0.134 and 0.446, respectively, there was a 19 % increase in peak load and a 27 % increase in the energy absorbed for the auxetic laminate in comparison to the non-auxetic laminate under quasi-static indentation tests.

In addition to indentation and impact, for the first time, we show that the stability of the composite laminates can be enhanced by introducing auxeticity. Fig. 1 shows schematics of auxetic composite laminates subjected to uniaxial compression under two conditions, one with two unloaded edges (*i.e.,* left and right edges) being free (see Fig. 1**(a)**) and the other with the two unloaded edges being simply supported (see Fig. 1**(b)**). For both schematics, the dashed line represents the original undeformed shape, and the solid line represents the deformed shape. Unlike traditional non-auxetic materials which expand in the lateral direction, the auxetic composite laminate contracts in the lateral direction when the two unloaded edges are free, producing compressive strain in the lateral direction (Fig. 1**(a)**), as indicated by the pink arrows where the length of the arrow represents the magnitude of the compressive strain. The aggregation of the compressive strains in the center of the auxetic composite produces a local material densification effect, which is expected to enhance the stability (*i.e.,* improved buckling resistance). When the two unloaded edges are simply supported (Fig. 1**(b)**), the uniaxial compression produces tensile strain (yellow arrows) only in the vicinity of the unloaded edges whereas primarily compressive strain in regions away from the two edges. A similar local material densification is expected as the compressive strain forces the material to flow into the center of the laminate, thereby enhancing the stability.

In authors' prior work [16], it was found through both experiments and FEA predictions that the critical buckling load of an auxetic CFRP composite laminate is about three times higher than that of an equivalent non-auxetic laminate under uniaxial compression and with free unloaded edges. Despite the enhancement in the buckling load that has

* Corresponding author.
E-mail address: ywang261@syr.edu (Y. Wang).

https://doi.org/10.1016/j.tws.2024.112409
Received 6 March 2024; Received in revised form 1 September 2024; Accepted 1 September 2024
Available online 2 September 2024

been observed in the experiments, it remains fundamentally unclear if such an improvement is really due to the auxeticity (*i.e.,* negative Poisson's ratio) or just simply caused by the change in the bending stiffness matrix (**D** matrix) as the composite layup changes. This ambiguity results from the fact that the **D** matrix normally governs the buckling strength of composite laminates [17] and that, in order to produce the negative Poisson's ratio, the layup must be specially adjusted, which simultaneously modifies the **D** matrix. Solving such a fundamental question is not only important to prevent the misinterpretation about the influence of negative Poisson's ratio on the stability of composites, but also crucial for many related studies on composites that look into the performance gains of adding auxeticity (*e.g.,* energy absorption [10,18], translaminar fracture toughness [19]). However, since the auxeticity and the **D** matrix change are tightly coupled, it is difficult to separate the auxeticity effect from the concurrent **D** matrix change. To solve this challenge, in this study, we developed and utilized a novel approach based on a homogeneous monoclinic plate with matched **D** matrix as the composite laminate to theoretically prove the role of negative Poisson's ratio in enhancing the buckling strength of composite laminate.

2. Uniaxial compression buckling test

The CFRP composite plates used in the current study were manufactured by sandwiching each IM7/977–3 carbon fiber prepreg tape layup between upper and lower caul plates, inserting the assembly into an autoclave, and following the manufacturer's recommended cure cycle. Upon demolding, both laminate types exhibited a very slight warpage (<1 mm of lift) on their two corners along the −45° diagonal. This occurred due to excess resin along the edges of the caul plate. This area was removed by trimming off 12 mm strips along the four edges of both laminates. Each laminate had an as-manufactured thickness of 0.7 mm, from which 139.7 mm long by 30 mm wide specimens were cut.

Fig. 2**(a)** shows the setup for the uniaxial compressive buckling test. The test fixture of the uniaxial compression buckling test is mounted in a servo-hydraulic MTS load frame. The upper and lower base plates have flat surfaces which impose a uniform shortening displacement across the specimen's width. The upper and lower surfaces also contain slide plates to further ensure out-of-plate alignment of the fixtures, as annotated in Fig. 2**(a)**. Prior to each test, the slide plates were tightened against the front and back faces of the specimen and bolted down as shown. The slide plates also locally constrained displacements in z and rotations about the x and y-axes, which corresponds to fixed-fixed boundary conditions along the top and bottom edges. Three specimens of each type (auxetic and non-auxetic) were tested.

Fig. 2**(b)** shows a typical load *vs*. displacement curve. Moduli were determined from the initial linear portion of the curve, and the straight-line intersection method [20,21] was used for the determination of the critical load (buckling strength). As illustrated, this method utilizes the point of intersection between two straight lines fitted to the linear portions of the loading and post-buckling paths and allows for an unambiguous definition of the critical load.

3. Buckling load predictions

A finite element (FE) model was created to predict critical buckling loads using the general-purpose FE software, ABAQUS. The model setup and the associated mesh is shown in Fig. 3**(a)**, where the composite laminate was modeled using two-dimensional shell elements. Fixed end boundary conditions were utilized that replicated those of the experimental setup. A unit shell edge load of 1 N/mm was applied, which distributes the load equally along the upper edge nodes. The model was used to compute load per unit width eigenvalues. The critical buckling load was taken as the lowest predicted eigenvalue multiplied by the specimen's width of 30 mm. Fig. 3**(b)** shows the example Shell General Stiffness module in the FE model, which uses the **A** (MPa•mm), **B** (MPa•mm^2), and **D** (MPa•mm^3) matrices for defining the laminate stiffness and allows for individual elements to be varied and investigated independently.

4. Effective in-plane and flexural properties

Fig. 4**(a)** shows the layups of the considered composite laminates, where [15/65/15/65/15] allows the laminate to produce negative effective Poisson's ratios of −0.41 (in-plane) and −0.37 (flexural) while [35/60/−5/60/35] allows the laminate to produce positive effective

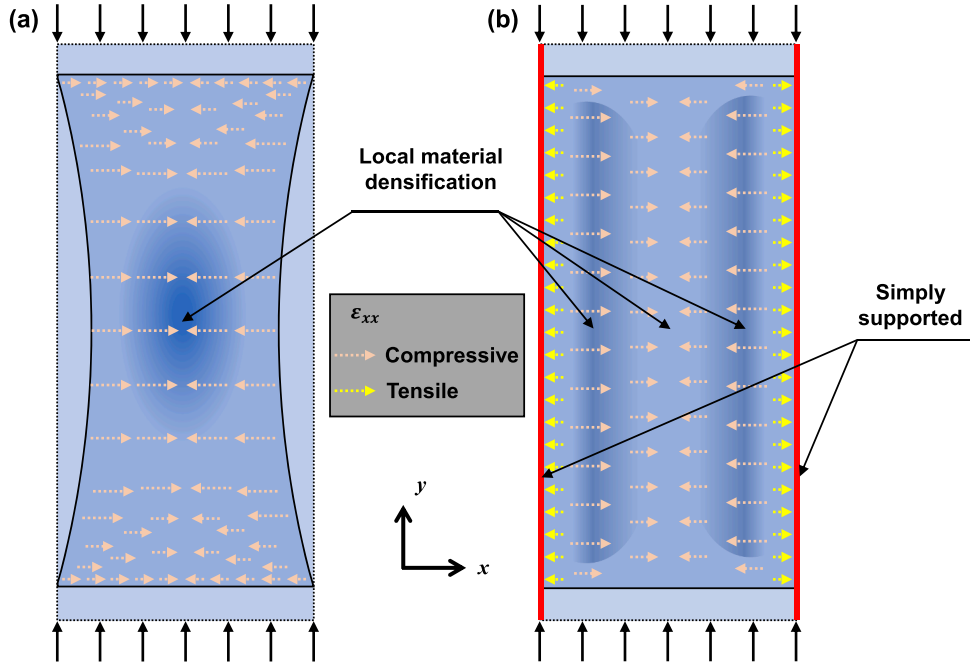

Fig. 1. Schematics of local material densification in auxetic composite laminates subjected to uniaxial compression with two unloaded edges (*i.e.,* left and right edges) being: (a) free and (b) simply supported.

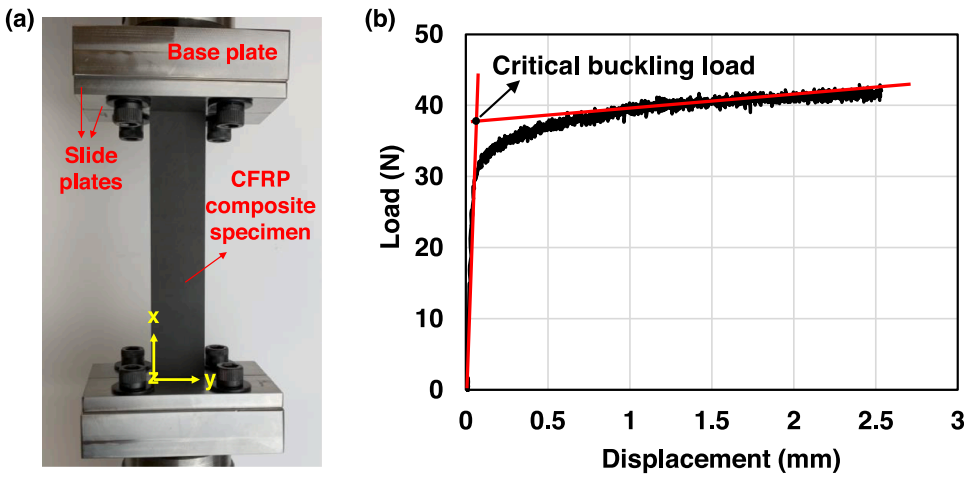

Fig. 2. (a) Setup for the uniaxial compressive buckling test, (b) buckling strength determination by the straight-line intersection method.

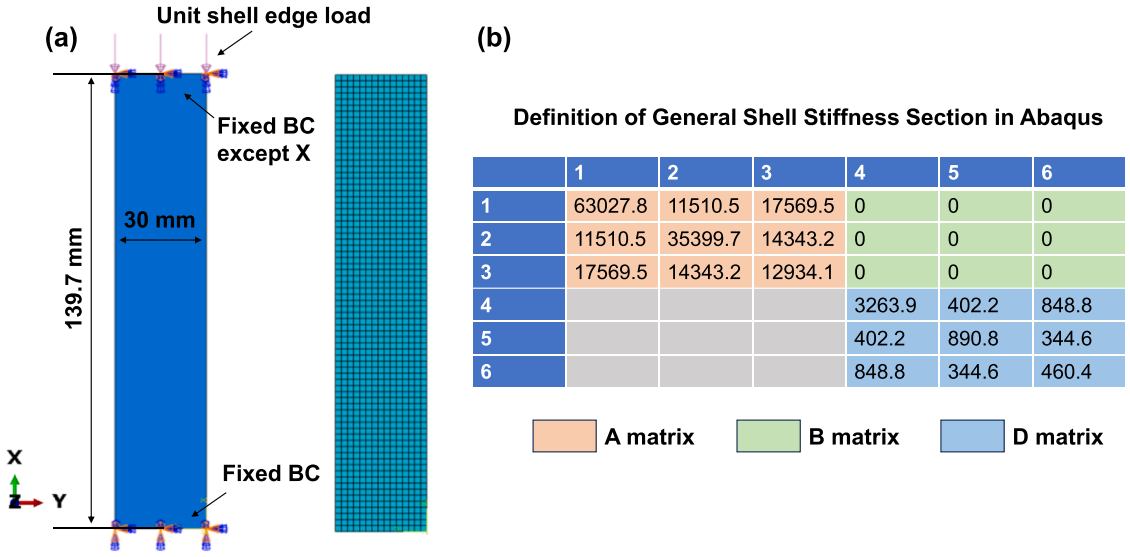

	1	2	3	4	5	6
1	63027.8	11510.5	17569.5	0	0	0
2	11510.5	35399.7	14343.2	0	0	0
3	17569.5	14343.2	12934.1	0	0	0
4				3263.9	402.2	848.8
5				402.2	890.8	344.6
6				848.8	344.6	460.4

Fig. 3. (a) The FEA model setup of compressive buckling analysis and the associated mesh, (b) an example Shell General Stiffness module in ABAQUS.

Poisson's ratios of 0.16 (in-plane) and 0.06 (flexural). These effective Poisson's ratios are those exhibited macroscopically at the laminate-level under in-plane and flexural loads. Specifically, the in-plane Poisson's ratio, ν^e_{12-i}, couples the longitudinal and transverse strain, and the flexural Poisson's ratio, ν^e_{12-f}, couples the bending in one direction and the transverse curvature in the perpendicular direction. These laminate-level effective Poisson's ratios along with the effective moduli can be calculated by the classical lamination theory using the extensional stiffness matrix (*i.e.,* **A** matrix) and the bending stiffness matrix (*i.e.,* **D** matrix), as discussed below.

From the **A** matrix, the in-plane effective properties, or the apparent mechanical properties of a laminate under in-plane loading, can be expressed in terms of the inverse of the **A** matrix as shown below:

$$E^e_{1-i}=\frac{1}{(ha_{11})},\quad E^e_{2-i}=\frac{1}{(ha_{22})},\quad \nu^e_{12-i}=-\frac{a_{21}}{a_{11}},$$
$$G^e_{12-i}=\frac{1}{(ha_{66})},\quad \nu^e_{16-i}=-\frac{a_{16}}{a_{11}},\quad \nu^e_{26-i}=-\frac{a_{26}}{a_{22}}, \tag{1}$$

where h is thickness of the composite laminate, a_{ij} is the element in the inverse of the extensional stiffness matrix ($\boldsymbol{a}=\boldsymbol{A}^{-1}$).

Similarly, the flexural effective properties, or the apparent mechanical properties of a laminate under flexural loading, can be expressed in terms of the inverse of the **D** matrix as shown below:

$$E^e_{1-f}=\frac{12}{(h^3d_{11})},\quad E^e_{2-f}=\frac{12}{(h^3d_{22})},\quad \nu^e_{12-f}=-\frac{d_{21}}{d_{11}},$$
$$G^e_{12-f}=\frac{12}{(h^3d_{66})},\quad \nu^e_{16-f}=-\frac{d_{16}}{d_{11}},\quad \nu^e_{26-f}=-\frac{d_{26}}{d_{22}}, \tag{2}$$

where d_{ij} is the element in the inverse of the bending stiffness matrix ($\boldsymbol{d}=\boldsymbol{D}^{-1}$).

The ply-level engineering constants of the IM7/977–3 prepreg are shown in Table 1 below, using which the **A** and **D** stiffness matrices of the auxetic and non-auxetic composite laminates can be calculated. These matrices can then be used to determine the laminate-level effective in-plane and flexural properties according to Eqs. (1) and (2).

Fig. 4**(b)** illustrates the comparison of the critical buckling load between the auxetic (116 ± 7.2 N) and non-auxetic (38 ± 1.1 N) CFRP composite laminates under uniaxial compression with two free unloaded edges. It also shows the comparison between the experimental data and the prediction from a traditional eigenvalue analysis using FEA (see Section 3), where close agreement can be observed. Moreover, the buckling mode predicted from FEA also compares favorably with that observed from the experimental test, as shown in Fig. 4**(c)**.

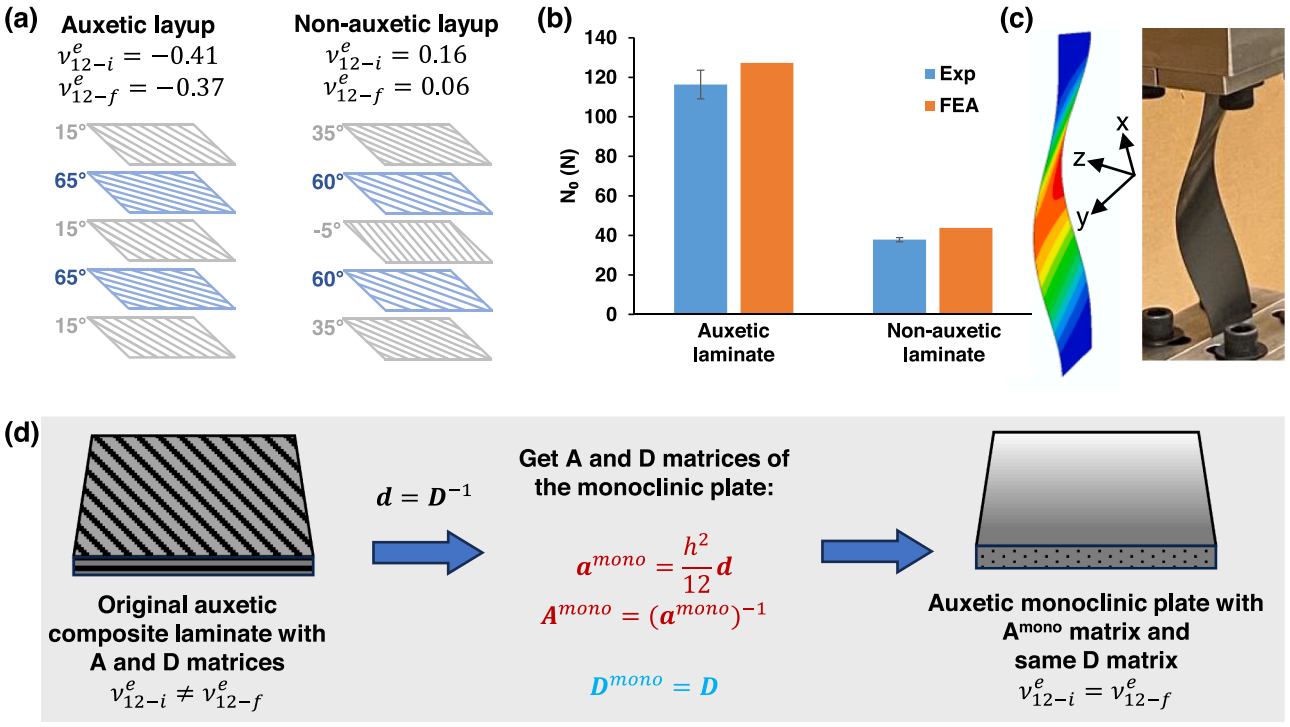

Fig. 4. (a) A comparison of in-plane and flexural Poisson's ratios for auxetic and non-auxetic layups of the composite laminates, (b) obtained critical buckling load auxetic laminate *vs.* non-auxetic laminate, (c) a comparison of the buckling shape between FEA prediction and experimental observation for the auxetic laminate, (d) steps of converting a composite laminate to an equivalent monoclinic plate.

Table 1
IM7/977-3 ply-level engineering constants [22-24].

Single ply thickness (mm)	Elastic moduli (GPa)	Ply-level Poisson's ratios
0.140	$E_{11} = 159$, $E_{22} = E_{33} = 9.20$ $G_{12} = G_{13} = 4.37$, $G_{23} = 2.57$	$\nu_{12} = \nu_{13} = 0.253$, $\nu_{23} = 0.456$

5. Monoclinic plate-based composite laminate approach

This section addresses the necessity and rationale of the monoclinic plate-based approach used in the current study. First, the intuitive way to demonstrate how a negative Poisson's ratio affects the buckling strength of composites would be to hold all other effective properties (E^e_1, E^e_2, G^e_{12}, ν^e_{16}, and ν^e_{26}) constant and adjust only the effective Poisson's ratio (ν^e_{12}). This is essentially unfeasible, though, since modifying the layup leads to concurrent changes for all other effective properties along with the effective Poisson's ratio. One alternative method is to manually alter the individual elements in the **D** matrix and then observe how such changes affect the overall data trends of the buckling strength between the auxetic and non-auxetic composite laminates. The attribution from the negative Poisson's ratio is indicated if the buckling strength substantially departs from each other or from their original trends. Moreover, changing the **D** matrix elements may force the effective Poisson's ratio to change from positive to negative (or vice-versa), and hence, influence the original data trends of the buckling strength, indicating the potential impact from the negative Poisson's ratio.

To utilize the above alternative method, there are two obstacles that must be overcome first. The first one is that although changing the individual element of the **D** matrix can change the flexural effective Poisson's ratio (*i.e.*, $\nu^e_{12-f} = -d_{21}/d_{11}$, where $\boldsymbol{d}$ is the inverse of the **D** matrix) from negative to positive (or *vice versa*), the in-plane effective Poisson's ratio (*i.e.*, $\nu^e_{12-i} = -a_{21}/a_{11}$, where $\boldsymbol{a}$ is the inverse of the **A** matrix) will stay negative or positive since the **A** matrix remains unchanged. For example, the auxetic layup of [15/65/15/65/15] allows to produce a negative in-plane effective Poisson's ratio of −0.41 and a negative flexural effective Poisson's ratio of −0.37 (see Fig. 4**(a)**). If we change the individual elements in the **D** matrix to manually change the flexural effective Poisson's ratio from −0.37 to a positive value, the in-plane effective Poisson's ratio remains unchanged at −0.41. Such a contradictory situation will cause confusion and makes it difficult to interpret the true influence of the negative Poisson's ratio on the observables (*i.e.,* the buckling strength in this context). The second obstacle is that changing the **D** matrix while holding the **A** matrix constant ($\boldsymbol{B} = 0$ for symmetric laminates) will result in a fictitious laminate, which may not be physically achievable.

To overcome the above-mentioned two challenges, a monoclinic plate-based composite laminate approach is proposed. The unique feature of a homogeneous monoclinic plate is that the in-plane effective properties are identical to the flexural effective properties. Therefore, creating a monoclinic plate with a matched **D** matrix with the auxetic composite laminate will result in an identical in-plane and flexural negative Poisson's ratio and a synchronous change from negative to positive when the **D** matrix is altered. Fig. 4**(d)** shows the flow chart of the steps involved in creating a monoclinic plate with a matched **D** matrix from a base composite laminate (*i.e.,* $\mathbf{D}^{mono} = \mathbf{D}$, where the superscript "mono" represents the monoclinic plate). To achieve this, the **A** matrix of the monoclinic plate, $\mathbf{A}^{mono}$, is obtained by the inverse of the $\boldsymbol{a}^{mono}$, where $\boldsymbol{a}^{mono} = h^2\boldsymbol{d}/12$, h is the thickness of the composite laminate, and $\boldsymbol{d}$ is the inverse of the **D** matrix. Substituting the corresponding elements of the newly obtained $\boldsymbol{a}^{mono}$ in Eq. (1) will lead to matched in-plane properties and flexural properties. Table 2 shows the calculated in-plane and flexural effective properties as well as **D** matrix elements of the auxetic composite laminate ([15/65/15/65/15]) (*i.e.,* before conversion to the monoclinic plate) and the created auxetic monoclinic plate (*i.e.,* after the conversion, denoted as "Aux").

As shown in Table 2, the conversion allows the monoclinic plate to retain all flexural effective properties, including the Poisson's ratio of

Table 2
Predicted effective moduli, Poisson's ratios, and nondimensional groups of the **D** matrix.

Property	Auxetic composite laminate [15/65/15/65/15]	Auxetic monoclinic plate ("Aux")	Non-auxetic counterpart monoclinic plate ("NA")
E^e_{1-i} (GPa)	51.29	56.44	56.63
E^e_{2-i} (GPa)	25.53	21.02	21.09
ν^e_{12-i}	−0.41	−0.37	0.36
E^e_{1-f} (GPa)	56.44	56.44	56.63
E^e_{2-i} (GPa)	21.02	21.02	21.09
ν^e_{12-f}	−0.37	−0.37	0.36
D_{11} (GPa·mm^3)	3.26	3.26	3.26
D_{16} /D_{11}	0.26	0.26	0.26
D_{26} /D_{11}	0.11	0.11	0.11
D_{22} /D_{11}	0.27	0.27	0.27
$(D_{12} + 2D_{66})$ /D_{11}	0.41	0.41	0.55

the original composite laminate, while at the same time, equating the flexural effective properties to the in-plane effective properties. In other words, the in-plane and flexural effective properties, including the Poisson's ratios are matched for the auxetic monoclinic plate. Note that the monoclinic plate does not represent the layup of the original composite laminate. It is created separately to study how the negative Poisson's ratio affects the buckling strength. Therefore, it is conceivable that the predicted critical buckling load of monoclinic plate from FEA will not match the experimental data in Fig. 4**(b)**.

To discern the effect of auxeticity *versus* changes in the elements themselves on the buckling load, the elements of the **D** matrix can then be varied independently, as this can be considered as simply choosing a different monoclinic material. Given the universe of layups, materials, and laminate thicknesses of the composite laminates, it is clear that the stacking sequences of the composite laminate counterpart can be physically achieved for each case considered.

To conclusively establish the dependence or independence of the critical buckling load (N_0) on the sign of the effective Poisson's ratio, a counterpart laminate was required where all **D** matrix elements were essentially the same, but with a very slight difference such that one was auxetic and one was not. From preliminary FEA results, it was observed that increasing only the D_{12} element for the auxetic plate from 0.4022 GPa-mm^3 to 0.8609 GPa-mm^3 would produce a monoclinic plate with an identical buckling load (under the *free unloaded edge* condition and with an aspect ratio of 0.2) that would be non-auxetic and which would have the same values of all other **D** matrix elements as the auxetic plate. This plate is denoted as "NA", which provided yet another starting point for variations in each **D** matrix elements. This proposed new approach provides a unique tool to discern the effect of auxeticity from the concurrent change in the **D** matrix as the composite layup changes, which cannot be achieved using the traditional one-parameter-at-a-time method.

It is worth stressing that, to the authors' knowledge, past studies have only looked at the effect of different stacking sequences of composite laminates on variations in the buckling strength (*e.g.,* [17,25]), which required the simultaneous change of all elements in the **D** matrix. Conversely, the current approach allows the effects of the individual **D** matrix elements to be isolated from the auxeticity effect. Specifically, four elements are individually changed including D_{16}, D_{26}, D_{22}, and $(D_{12} + 2D_{66})$, which correspond to the four coefficients of the governing equation of the instability of a composite laminate [17].

6. Results

The stability of composite laminates is highly sensitive to the boundary conditions and the aspect ratio of the plate (*i.e., a/b*, where *a* is the length and *b* is the width of the plate). The effect of auxeticity due to the local material densification phenomenon could be triggered or augmented as the boundary conditions and the aspect ratio of the plate change, which is evidenced in the results presented in Figs. 5-8. Specifically, Figs. 5 and 6 present the buckling results for the auxetic and non-auxetic monoclinic plates with unloaded edges being free and simply supported, respectively, while holding the aspect ratio constant at $a/b = 0.2$. Figs. 7 and 8 show the results for those having an aspect ratio of $a/b = 1$. These results were obtained from the validated eigenvalue analysis using FEA by individually changing the **D** matrix elements. By observing the effects of respective modifications on the overall data trends of obtained buckling strength, the attribution from the negative Poisson's ratio can be indicated if the buckling strength substantially departs from each other or from their original trends. Numerically, this was achieved by assigning a Shell General Stiffness section to a 2D shell plate using the general-purpose FEA software ABAQUS, which allowed for the manual entry of stiffness matrix values (including $\mathbf{A}^{mono}$, $\mathbf{B}^{mono}$, and **D** matrices, where $\mathbf{B}^{mono} = 0$ for symmetric laminates) while maintaining the matrices' positive definiteness (see Fig. 3**(b)**).

Results in Fig. 5 demonstrate that when the monoclinic plate or the composite laminate has an aspect ratio of $a/b = 0.2$, auxeticity has no intrinsic effect on buckling strength under uniaxial compression with free unloaded edges. Figs. 5**(a)** - 5**(d)** illustrate how the normalized critical buckling load of the auxetic and non-auxetic plates is affected by the change in the nondimensional **D** matrix elements. In these figures, the black discrete dots denote the original auxetic and non-auxetic monoclinic plates where the **D** matrices were un-altered (*i.e.,* exactly same with those in Table 2) while the red discrete dots represent cases where auxetic monoclinic plates ($\nu^e_{12} < 0$) that became non-auxetic ($\nu^e_{12} > 0$) due to the change of the individual elements in **D** or vice-versa. The same annotation format was employed in Figs. 6-8. Note here the critical buckling load, N_0, has a unit of N/mm, after normalization by the D_{11} element of bending stiffness matrix, the normalized critical buckling load has a unit of 1/mm^2 as shown in the vertical axes for Figs. 5-8.

In Fig. 5**(a)**, although slight difference is observed, the normalized buckling load follows the same trend for both the auxetic and non-auxetic plates with the change of D_{16}/D_{11}. For the auxetic plate, there are two red discrete dots at $D_{16}/D_{11} = 0.10$ and $D_{16}/D_{11} = 0.15$, which indicate cases where the auxetic plate became non-auxetic due to the change in the D_{16} element. As one can see, there is no change in the data trend for the auxetic plate with varying D_{16} when the auxetic case becomes non-auxetic. The normalized buckling load matched between the auxetic and non-auxetic plates at $D_{16}/D_{11} = 0.26$, which is expected as the **D** matrix of the non-auxetic plate was deliberately designed to match the critical buckling load (see Section 4). A similar pattern can be observed in Fig. 5**(b)**, where the auxetic plate became non-auxetic at $D_{26}/D_{11} = 0.05$ and the non-auxetic plate became auxetic at $D_{26}/D_{11} = 0.17$ and $D_{26}/D_{11} = 0.18$. Such changes have not resulted in any noticeable changes in the data trends for either plate type. In Fig. 5**(c)**, the auxetic and non-auxetic results virtually coincide as the D_{22}/D_{11} changes. No cases were found where auxetic becomes non-auxetic or *vice versa*. In Fig. 5**(d)**, the normalized buckling load for the original auxetic case and non-auxetic case does not overlap, which is expected since the D_{12} element is different for the two cases (*i.e.,* $D_{12} = 0.4022$ GPa-mm^3 for auxetic and $D_{12} = 0.8609$ GPa-mm^3 for non-auxetic). Two configurations were taken into consideration for changing the nondimensional group of $(D_{12} + 2D_{66})/D_{11}$: one configuration fixed D_{12} and merely varied D_{66}, while the second configuration was the opposite. For the first configuration, several cases exist where the auxetic case becomes non-auxetic or *vice versa*. Nevertheless, the data trend remains and the differences between auxetic and non-auxetic stay the same as the nondimensional group changes. For the second configuration, the range of the nondimensional group of $(D_{12} + 2D_{66})/D_{11}$ over which the variations of

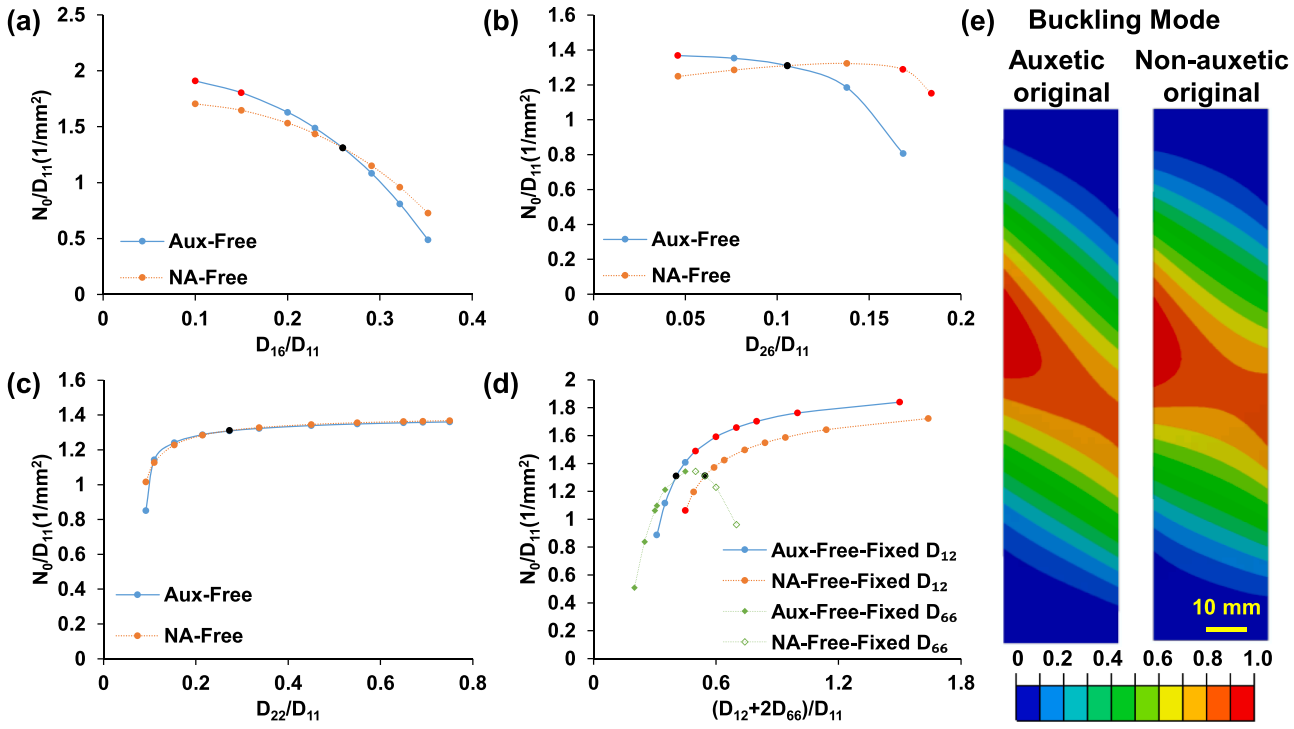

Fig. 5. Response of normalized critical buckling load under varying (a) $\frac{D_{16}}{D_{11}}$, (b) $\frac{D_{26}}{D_{11}}$, (c) $\frac{D_{22}}{D_{11}}$, and (d) $\frac{(D_{12}+2D_{66})}{D_{11}}$ ratios at plate *aspect ratio of* $a/b = 0.2$ and *free unloaded edges*. (e) a comparison of the predicted buckling mode between the original auxetic and non-auxetic monoclinic plates with unaltered **D** matrices.

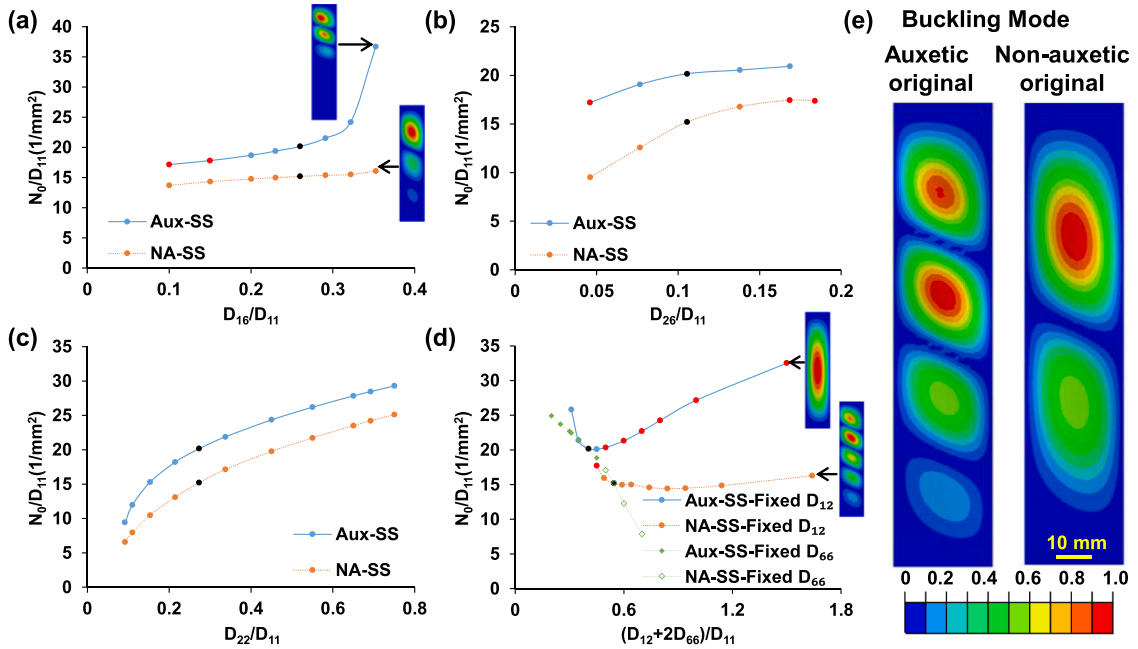

Fig. 6. Response of normalized critical buckling load under varying (a) $\frac{D_{16}}{D_{11}}$, (b) $\frac{D_{26}}{D_{11}}$, (c) $\frac{D_{22}}{D_{11}}$, and (d) $\frac{(D_{12}+2D_{66})}{D_{11}}$ ratios at plate aspect ratio of $a/b = 0.2$ and simply supported unloaded edges. (e) a comparison of the predicted buckling mode between the original auxetic and non-auxetic monoclinic plates with unaltered **D** matrices.

the normalized buckling load occur is different for the two sets of plates due to the limitation of the positive definiteness of the **D** matrix while varying the individual D_{12}. Hence, such a comparison does not yield any conclusive findings. Fig. 5**(e)** shows a comparison of the buckling mode between the original auxetic and non-auxetic plates, where an identical pattern can be observed. A similar identical comparison can also be found for cases where the **D** elements vary. The combination of observations leads to the conclusion that auxeticity has no intrinsic effect on buckling strength of the monoclinic plate with an aspect ratio of $a/b = 0.2$ under uniaxial compression with free unloaded edges. Rather, the differences in the buckling strength are due to differences in the elements of the **D** matrix and the way that they interact to affect the critical buckling load.

When the boundary condition of the two unloaded edges were

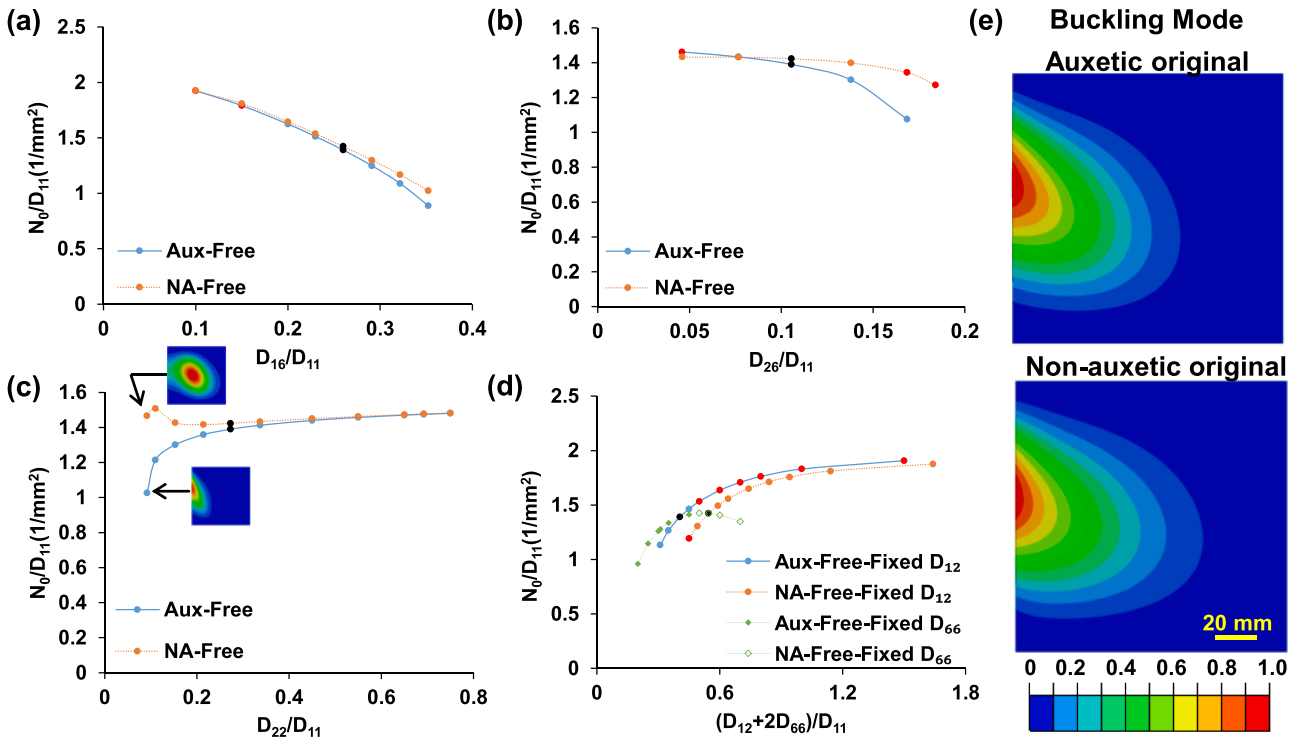

Fig. 7. Response of normalized critical buckling load under varying (a) $\frac{D_{16}}{D_{11}}$, (b) $\frac{D_{26}}{D_{11}}$, (c) $\frac{D_{22}}{D_{11}}$, and (d) $\frac{(D_{12}+2D_{66})}{D_{11}}$ ratios at plate *aspect ratio of* $a/b = 1$ and *free unloaded edges*. (e) a comparison of the predicted buckling mode between the original auxetic and non-auxetic monoclinic plates with unaltered **D** matrices.

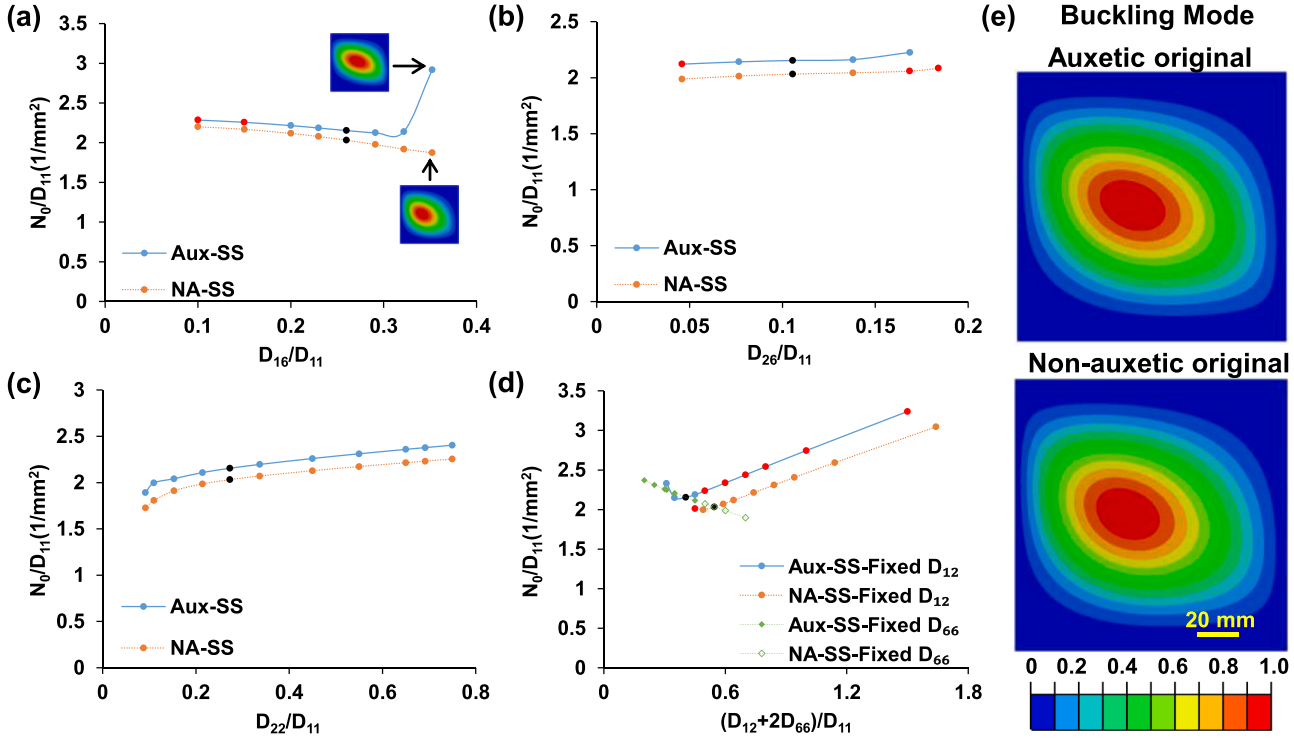

Fig. 8. Response of normalized critical buckling load under varying (a) $\frac{D_{16}}{D_{11}}$, (b) $\frac{D_{26}}{D_{11}}$, (c) $\frac{D_{22}}{D_{11}}$, and (d) $\frac{(D_{12}+2D_{66})}{D_{11}}$ ratios at plate aspect ratio of $a/b = 1$ and simply supported unloaded edges. (e) a comparison of the predicted buckling mode between the original auxetic and non-auxetic monoclinic plates with unaltered **D** matrices.

changed to simply supported, the enhancement effect due to auxeticity (*i.e.,* local material densification) is evident and started to provide enhancement in the buckling strength, as shown in results in Fig. 6. In Fig. 6**(a)**, it shows that the overall data trend of the normalized buckling load of the auxetic plate is largely different from that of the non-auxetic one. Specifically, the non-auxetic plate showed only a slight increase as

the D_{16}/D_{11} increases, whereas the auxetic plate showed a mild increase first at lower D_{16}/D_{11} ratios and exhibited an abrupt jump when D_{16}/D_{11} reaches near 0.3. The difference between the auxetic and non-auxetic plates continuously increases as the D_{16}/D_{11} increases. This signifies that the auxetic monoclinic plate and composite laminate, if designed with a larger D_{16}/D_{11}, *i.e.,* physically more bending-twisting coupling, will receive benefit from the auxeticity effect, resulting in substantially improved buckling strength. The buckling modes of the auxetic and non-auxetic monoclinic plate at $D_{16}/D_{11} = 0.35$ are annotated in Fig. 6**(a)**, where it can be seen that the buckling pattern (*i.e.,* the out-of-plane deflection) of the auxetic plate is more concentrated in the upper half whereas the buckling pattern of the non-auxetic plate is more dispersed over the whole plate. The same apparent enhancement effect has not been observed in Figs. 6**(b)** and 6**(c)**, indicating that the negative Poisson's ratio effect remains inactive as the D_{26}/D_{11} and D_{22}/D_{11} change. Although there are a few cases where the auxetic case became non-auxetic and *vice versa* in Fig. 6**(b)**, they did not influence the overall data trend of either the auxetic or the non-auxetic case.

Similarly, the auxeticity effect appears to stay inactive as the nondimensional group $(D_{12}+2D_{66})/D_{11}$ changes, specifically for the configuration where D_{66} was fixed and D_{12} was allowed to vary. The normalized buckling load shows a continuously decreasing trend regardless of the change in auxeticity, as shown in Fig. 6**(d)**. For the opposite configuration where D_{12} was fixed and D_{66} was allowed to vary, the results were inconclusive. Although the data trends between the auxetic and non-auxetic plates appear to be largely different, especially for the data located on the right side of the black dots, most of the auxetic cases were found to have been converted from auxetic to non-auxetic due to the change of the D_{66}. The difference in the normalized buckling load in this context is likely caused by the shift in the buckling modes. For example, the non-auxetic plate converted from the originally auxetic plate showed a single sine wave whereas the non-auxetic plate varied from originally non-auxetic showed multiple sine waves, as annotated in Fig. 6**(d)**. In addition, the enhancement effect due to auxeticity can also be gleaned by comparing the buckling modes between the original auxetic and non-auxetic plates, as shown in Fig. 6**(e)**, where the auxetic plate showed four sine waves due to local material densification whereas the non-auxetic plate showed only two.

The enhancement effect due to auxeticity is not only active when a simply supported boundary condition is imposed on the unloaded edges, it can also be triggered for cases where the unloaded edges are set free but with an increased plate aspect ratio of $a/b = 1$, as shown in Fig. 7. First, the auxeticity effect on the enhancement of the buckling strength was not evident in Figs. 7**(a) and 7(b)**, where the normalized buckling load of auxetic and non-auxetic plates tend to vary similarly to each other with the change of D_{16}/D_{11} and D_{26}/D_{11}, even for cases where auxetic changed to non-auxetic or *vice versa*. The enhancement effect due to auxeticity became obvious in Fig. 7**(c)**, where the normalized buckling load exhibited a large difference in the data trend between the auxetic and non-auxetic plates on the left side of the black dots (*i.e.,* the original auxetic and non-auxetic plates with un-altered **D** matrices) with the change of D_{22}/D_{11}. Specifically, the auxetic plate generally showed a decreasing trend starting from a high normalized buckling load whereas the non-auxetic plate displayed a rising trend beginning from a relatively much lower load. The buckling modes of the two cases are also distinct as annotated in Fig. 7**(c)**, where the buckling pattern is dispersed across the entire plate in the auxetic plate whereas the buckling pattern is more concentrated on the left edge in the non-auxetic plate. When the data approached the black dots, both the auxetic and non-auxetic began to plateau and gradually coincide with each other. This physically shows that the auxeticity effect for enhancing the buckling strength can be triggered by lowering the D_{22}/D_{11}, which is the anisotropy of the bending stiffness between the longitudinal and the lateral directions. The auxeticity effect was not observed in Fig. 7**(d)**, where changing the nondimensional group $(D_{12}+2D_{66})/D_{11}$ in either configuration has not led to any noticeable difference in the data trends between the auxetic and non-auxetic plates, although a few auxetic cases became non-auxetic and one non-auxetic case turned to auxetic. A comparison of the buckling pattern between the original auxetic and non-auxetic plates (where **D** matrices were un-altered) is provided in Fig. 7**(e)**. It shows that the two buckling patterns are identical, indicating no direct enhancement effect due to auxeticity in the original configuration.

The auxeticity effect for enhancing the buckling load persists as the boundary condition of the two unloaded edges were switched to simply supported for plates having an aspect ratio of $a/b = 1$. Fig. 8 depicts the comparison of buckling results between the auxetic and non-auxetic monoclinic plates. The enhancement effect due to the auxeticity is clearly observed in Fig. 8**(a)**, where the data trends of the auxetic and non-auxetic plates are initially similar but significantly deviate from each other as the D_{16}/D_{11} exceeds 0.35. As one can see, the normalized buckling load of the auxetic plate drastically departed from the original data trend and increases whereas that of the non-auxetic plate remained on the original data trend. This indicates that the auxeticity effect clearly became active as the D_{16}/D_{11} exceeds the threshold. A composite laminate, if designed with a higher D_{16}/D_{11} ratio (*i.e.,* higher bending-twisting coupling), is expected to gain enhancement in the stability under uniaxial compression. Interestingly, the auxetic and non-auxetic plates show similar buckling patterns for cases where the data trends depart from each other. This implies that the auxeticity did not result in any significant changes to the buckling mode, but rather, the enhancement in the buckling strength could be due to the unique local material densification effect as shown in Fig. 1**(b)**. The same enhancement effect in the buckling load due to auxeticity was not observed in Figs. 8**(b)**–8**(d)**. It can be seen that the data trends remain virtually similar to each other as D_{26}/D_{11}, D_{22}/D_{11}, and the nondimensional group of $(D_{12}+2D_{66})/D_{11}$ change. Furthermore, the buckling modes of the auxetic and non-auxetic plates are identical to each other, as compared in Fig. 8**(e)**, indicating no direct effect attributable to the auxeticity.

7. Discussion

The results presented above demonstrate that the auxeticity effect is highly sensitive to the individual bending stiffness matrix elements. The enhancement of the buckling strength due to the auxeticity from local material densification could be triggered, augmented, or diminished at varying individual stiffness matrix elements. Specifically, our results indicate that for buckling critical applications, composite laminates can be designed by increasing the bending-twisting ratio (*i.e.,* D_{16}/D_{11}) and decreasing the anisotropy of the bending stiffness between the longitudinal and lateral directions (*i.e.,* D_{22}/D_{11}) to trigger the auxeticity enhancement effect on the buckling strength. However, doing so inevitably necessitates the consideration of the manufacturing challenges because increasing the bending-twisting ratio could lead to warping issues, especially in relatively thin laminates, while lowering the anisotropy of the bending stiffness could indicate a modification in the material composition. These challenges merit further application-oriented studies.

It is worth mentioning that the results and the proposed approach in this study are not only important to understand the auxeticity effect on the enhancement of stability of the composite laminates, but also provide a unique capability to isolate the auxeticity effect from the concurrent change of the stiffness matrices. Applications that can benefit from this capability include comparisons of a layered composite structures' resistance to low velocity impact and quasi-static indentation damage. Traditionally, in those studies, composite laminates were chosen by either matching the effective values of E_3^e [5, 7, 8], E_1^e [15], or E_1^e and E_3^e [11, 12]. However, for such out-of-plane loadings, the values of **D** matrix elements are also important, with their importance increasing as the unsupported dimensions of the plate increase. Conclusions about the effects of auxeticity based only on matching effective engineering constants inevitably overlook these effects and attribute

them solely to auxeticity. Similar considerations can be applied to other loadings. For example, for tensile loading, elements of the **A** matrix may prove to be a better comparison method than through effective engineering constants.

8. Conclusion

Auxetic composite laminates were experimentally shown to outperform the equivalent non-auxetic laminates by three times in the critical buckling strength under uniaxial compression. To investigate whether such an enhancement effect is due to the negative Poisson's ratio (*i.e.,* auxeticity) or simply caused by the concurrent change of the bending stiffness matrix (*i.e.,* **D** matrix) as the layup changes, this study proposed a novel monoclinic plate-based composite laminate approach, which uniquely separates the auxeticity effect from the simultaneous change of the **D** matrix elements. Results from this study mainly lead to following conclusions:

The negative Poisson's ratio (*i.e.,* auxeticity) plays an active role in enhancing the critical buckling strength of composite laminates due to the local material densification phenomenon, where such a role is dynamically responsive to the **D** matrix elements. When the two unloaded edges of the composite laminates are simply supported, the auxeticity effect becomes active as the bending-twisting ratio (*i.e.,* D_{16}/D_{11}) increases. Whereas when the two unloaded edges are set free, the auxeticity effect is triggered as the anisotropy of the bending stiffness between the longitudinal and lateral directions (*i.e.,* D_{22}/D_{11}) decreases.

Results from this study are expected to provide useful guidance in exploiting the negative Poisson's ratio to design layered anisotropic composite structures for improved stability. The proposed approach also provides a unique capability of isolating the auxeticity effect from the concurrent changes in stiffness matrices, thereby unraveling the true auxeticity effect for other related studies that investigate the performance gains (*e.g.,* low velocity impact, indentation, fraction toughness) through introducing auxeticity.

CRediT authorship contribution statement

Wenhua Lin: Writing – original draft, Visualization, Validation, Investigation, Formal analysis, Data curation. **Yeqing Wang:** Writing – review & editing, Visualization, Validation, Supervision, Methodology, Investigation, Funding acquisition, Conceptualization. **Barry D. Davidson:** Writing – review & editing, Validation, Supervision, Methodology, Investigation.

Declaration of competing interest

The authors declare that they have no known competing financial interests or personal relationships that could have appeared to influence the work reported in this paper.

Data availability

Data will be made available on request.

Acknowledgments

The authors would like to acknowledge the financial support provided by National Science Foundation under Award No. CMMI-2202737

References

[1] J.I. Lipton, R. MacCurdy, Z. Manchester, L. Chin, D. Cellucci, D. Rus, Handedness in shearing auxetics creates rigid and compliant structures, Science (1979) 360 (6389) (2018) 632–635.
[2] K. Liu, R. Sun, C. Daraio, Growth rules for irregular architected materials with programmable properties, Science (1979) 377 (6609) (2022) 975–981.
[3] N.K. Choudhry, B. Panda, S. Kumar, Enhanced energy absorption performance of 3D printed 2D auxetic lattices, Thin-Walled Struct. 186 (2023) 110650.
[4] A. Alomarah, Y. Yuan, D. Ruan, A bio-inspired auxetic metamaterial with two plateau regimes: compressive properties and energy absorption, Thin-Walled Struct. 192 (2023) 111175.
[5] K.L. Alderson, V.R. Simkins, V.L. Coenen, P.J. Davies, A. Alderson, K.E. Evans, How to make auxetic fibre reinforced composites, Phys. Status Solidi (b) 242 (3) (2005) 509–518.
[6] Y. Fan, H.-S. Shen, Y. Xiang, Nonlinear vibration characteristics of pre-and post-buckled FG-GRMMC laminated plates with in-plane auxeticity, Eng. Struct. 274 (2023) 115068.
[7] K.L. Alderson, V.L. Coenen, The low velocity impact response of auxetic carbon fibre laminates, Phys. Status Solidi (b) 245 (3) (2008) 489–496.
[8] V.L. Coenen, K.L. Alderson, Mechanisms of failure in the static indentation resistance of auxetic carbon fibre laminates, Phys. Status Solidi (b) 248 (1) (2011) 66–72.
[9] S. Hou, T. Li, Z. Jia, L. Wang, Mechanical properties of sandwich composites with 3d-printed auxetic and non-auxetic lattice cores under low velocity impact, Mater. Des. 160 (2018) 1305–1321.
[10] T. Li, F. Liu, L. Wang, Enhancing indentation and impact resistance in auxetic composite materials, Compos. Part B: Eng. 198 (2020) 108229.
[11] W. Lin, Y. Wang, Low velocity impact behavior of auxetic CFRP composite laminates with in-plane negative poisson's ratio, J. Compos. Mater. 57 (12) (2023) 2029–2042.
[12] Y. Wang, Auxetic composite laminates with through-thickness negative Poisson's ratio for mitigating low velocity impact damage: a numerical study, Materials. (Basel) 16 (2022) 6963.
[13] L. Zhou, J. Zeng, L. Jiang, H. Hu, Low-velocity impact properties of 3D auxetic textile composite, J. Mater. Sci. 53 (5) (2018) 3899–3914.
[14] Y. Fan, Y. Wang, The effect of negative Poisson's ratio on the low-velocity impact response of an auxetic nanocomposite laminate beam, Int. J. Mech. Mater. Des. 17 (1) (2021) 153–169.
[15] S. Aziz, An Investigation Into the Post Impact and Post Indentation Behavior of Auxetic Composites, University of Bolton, 2016. PhD thesis.
[16] A. Tricarico, W. Lin, Y. Wang, High buckling strength of auxetic carbon fiber composite laminates, in: 38th Annual American Society for Composites Technical Conference, DEStech Publishing Inc., Boston, MA, 2023.
[17] J.M. Whitney, Structural Analysis of Laminated Anisotropic Plates, CRC Press, 1987.
[18] T. Allen, J. Shepherd, T.A.M. Hewage, T. Senior, L. Foster, A. Alderson, Low-kinetic energy impact response of auxetic and conventional open-cell polyurethane foams, Phys. Status Solidi (b) 252 (7) (2015) 1631–1639.
[19] J.P. Donoghue, K.L. Alderson, K.E. Evans, The fracture toughness of composite laminates with a negative Poisson's ratio, Phys. Status Solidi (b) 246 (9) (2009) 2011–2017.
[20] H. Debski, T. Kubiak, A. Teter, Buckling and postbuckling behaviour of thin-walled composite channel section column, Compos. Struct. 100 (2013) 195–204.
[21] Q.H. Doan, D.-K. Thai, N.L. Tran, A numerical study of the effect of component dimensions on the critical buckling load of a GFRP composite strut under uniaxial compression, Materials. (Basel) 13 (4) (2020) 931.
[22] X. Li, D. Ma, H. Liu, W. Tan, X. Gong, C. Zhang, Y. Li, Assessment of failure criteria and damage evolution methods for composite laminates under low-velocity impact, Compos. Struct. 207 (2019) 727–739.
[23] B. Mohammadi, M. Rohanifar, D. Salimi-Majd, A. Farrokhabadi, Micromechanical prediction of damage due to transverse ply cracking under fatigue loading in composite laminates, J. Reinf. Plast. Compos. 36 (5) (2017) 377–395.
[24] J. Zhang, X. Zhang, An efficient approach for predicting low-velocity impact force and damage in composite laminates, Compos. Struct. 130 (2015) 85–94.
[25] R.M. Jones, Mechanics of Composite Materials, CRC press, 1998.